IEEE Access
Multidisciplinary | Rapid Review | Open Access Journal

Received June 25, 2019, accepted July 13, 2019, date of publication July 17, 2019, date of current version August 15, 2019.

Digital Object Identifier 10.1109/ACCESS.2019.2929429

A Calculation Method for the On-Load Cogging Torque of Permanent Magnet Synchronous Machine

WEIYE WANG[1], (Student Member, IEEE), HUI MA[1], XIN QIU[1,2], AND JIANFEI YANG[1,2]
[1]School of Electrical and Automation Engineering, Nanjing Normal University, Nanjing 210046, China
[2]Jiangsu Key Laboratory of 3D Printing Equipment and Manufacturing, Nanjing 210042, China

Corresponding author: Xin Qiu (qiuxin_nh@163.com)

This work was supported in part by the National Natural Science Foundation of China under Award 51607094 and Award 51407095, in part by the Province Natural Science Foundation of Jiangsu, under Project BK20151548, in part by the Jiangsu "Six Talent Peaks" Project, under Project GDZB-043, in part by the Nanjing Post-Subsidy Program, under Project 201722046, and in part by the Postgraduate Research and Practice Innovation Program of Jiangsu Province, under Project KYCX19_0806.

ABSTRACT This paper presents a new method to calculate the cogging torque of the permanent magnet synchronous machine under load condition. Combined with the mathematical expression of the cogging torque, it is found that the cogging torque will be influenced by the load. In order to accurately analyze the torque ripple of the motor at low speed and high torque operation and make it possible to reduce the cogging torque under load condition, it is necessary to calculate the cogging torque accurately. A calculation method for the on-load cogging torque of the PMSM, which the cross magnetization and core saturation have been taken into consideration, is proposed in this paper. The finite element analysis (FEA) and field-oriented control (FOC) contribute to the method, which mainly consists of three parts: elimination of the reluctance torque, calculation of the average torque, and the ripple torque and the separation of the cogging torque. By using this method, the cogging torques of a 16-pole/24-slot PMSM under different load conditions has been calculated. The result shows a very good agreement between simulation and experiment, which verifies the feasibility and effectiveness of the proposed method.

INDEX TERMS Cogging torque, cross magnetization, core saturation, permanent magnet synchronous machine.

I. INTRODUCTION

Owing to the low loss and high torque density, permanent magnet synchronous machine (PMSM) have been widely used in military equipment, home and industrial applications [1]. However, the permanent magnet will cause the cogging torque, which will produce vibration and noise, and influence the control accuracy of the system. With the dual advantages of environmental protection and energy saving, the electric vehicle is the future urban transport system in the mobile element and PMSM is the most suitable for the electric vehicle owing to high torque density. However, the electric vehicle is frequently in a state of low speed and high torque in urban traffic environment, which means the impact of the cogging torque on the control performance of electric vehicle is very significant. In order to ensure the smooth operation of PMSM, many investigations have been carried out on the cogging torque [2]–[8].

Many previous papers were focused on the analysis of the influence of stator and rotor structure on the cogging torque of PMSM [9]–[14], such as the skewing technique [15], [16], different teeth widths [17], [18], slot-opening shift [19], the asymmetric angles of magnetic pole [20], pole-arc coefficient optimization [21], permanent magnet segmentation [22] and pole shape optimization [23]. However, when the motor is loaded, the magnetic saturation state is aggravated, and the cogging torque is not only affected by the stator and rotor structure, but also by the load. Because motor usually works under rated load, the analysis of the influence of load on the cogging torque is essential, and the calculation method of on-load cogging torque has become one of the current research hotspots of PMSM.

Under load condition, four components mainly contribute to the output torque of the PMSM: average torque, reluctance

The associate editor coordinating the review of this manuscript and approving it for publication was Gaolin Wang.

torque, waveform torque and cogging torque [24], [25]. The DC components of the output torque are the average torque and reluctance torque, which are both produced by the interaction of the permanent magnets and armature fields. And the ripple torque is the harmonic torque generated by the harmonic component of the back EMF. When machine is running with rated load or overload, the permanent magnets and armature fields influence each other and the remarkable local magnetic saturation appear at the inner surface of stator teeth and the outer surface of the rotor [26], [27]. The motor parameters such as the back EMF and inductance are inevitably varied by the magnitude and phase angle of the armature current [28]–[30]. The frozen permeability (FP) method is a commonly used method for calculating motor parameters under load conditions. The key component of the FP method is that the permeability of each element under load condition is fixed and used to resolve the model linearly without electric loading. With the utilization of the FP method, many investigations have been carried out to analysis the cogging torque under load conditions [31], [32]. In [33], the torque is decomposed into four components by using the FEA along with the frozen permeability technique, and the variations in the machine parameters and the torque components are discussed by using the flux distributions separated according to origins. In addition, the on-load cogging torque is separated from the output torque in [34], but the average of the calculated torque is not zero, which is not in accordance with the characteristics of the cogging torque. In order to accurately calculate the torque, an on-load cogging torque calculation method has been proposed in [35], which is based on the virtual work principle in conjunction with the FP method. Although previously proposed methods can relative accurately obtain the cogging torque under load conditions, and its disadvantage is also obvious that the methods require multiple FEAs and cannot be verified by experiments. Another method is proposed in [36], which is based on conformal mapping and magnetic equivalent circuits (CM-MEC) for on-load analysis of surface permanent magnet synchronous machine with integer slot and fractional slot windings. But the method needs to analyze the magnetic circuit, which is inconvenient to apply in practice. Hence, a method for on-load cogging torque calculation of PMSM, which has good robustness and the feasibility, is proposed in this paper.

In this paper, a PMSM with concentrated and fractional slot windings, which is a common motor structure, is used as an analysis model. First, the influence of the local magnetic field saturation on the cogging torque is analyzed by the FEA at rated-load condition. Next, a calculation method, which requires fewer FE calculations and is convenient to implement, is proposed for the on-load cogging torque of PMSM. During this procedure, the influence of the cross-magnetization on the permanent magnet field is analyzed and the elimination method of the reluctance torque is proposed by changing the phase of the phase current, which contribute to the calculation of the on-load cogging torque. Finally, the correlation between the cogging torque and the load is analyzed and the results of the analysis on the designed PMSM are compared with the measured results, which proves the availability of the proposed method.

II. ANALYSIS MODEL

In order to reveal the influence of the local magnetic field saturation and the cross-magnetization, as well as the accurate separation and analysis of the cogging torque under load, the investigations are carried out on a 24-slot/16-pole PMSM, whose cross section and parameters are given in Table 1 and Fig. 1. All the load conditions are simulated by injecting currents to the stator windings, and the three-phase currents have the same frequency, amplitude and phase difference (120 degree). In particular, the PMSM is in the state of no-load when the current is zero.

TABLE 1. Basic parameters of the investigated machine.

Parameters	value	Parameters	value
Stator outer diameter	140mm	Axial length	30mm
Stator inner diameter	88.6	Airgap length	0.8mm
Tooth width	7mm	Back iron thickness	8.5mm
Tooth-tip height	1.3mm	Turns per phase	56
Magnet thickness	3.3mm	Magnet pole arc	140°
Rated current(Peak)	17.5A	Stacking Factor	0.97
PM remanence	1.03T	PM permeability	$1.03\mu_0$

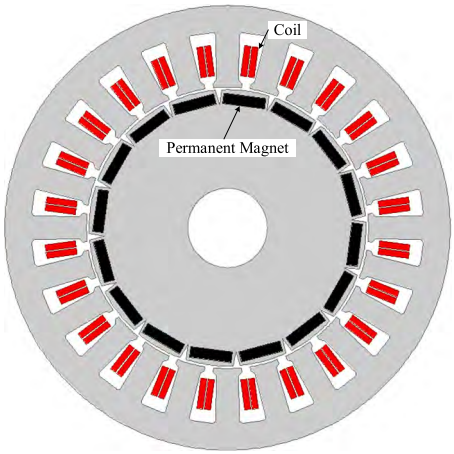

FIGURE 1. Cross section of the PMSM.

III. COGGING TORQUE ANALYSIS

Cogging torque is caused by the tangential component of the interaction force between permanent magnet and armature teeth, and it can be calculated by magnetic energy variation at no-load condition, which is shown as follow:

$$T_{cog(no-load)} = -\partial W_{no-load}/(\partial\theta) \tag{1}$$

where $W_{no-load}$ is the magnetic energy of the machine at no-load condition, θ is the position angle of the rotor.

To facilitate analysis, the following assumptions are made:

1) The permanent magnet is in the same magnetic permeability of air, and its magnetic energy is assumed to be constant;

2) All permanent magnets are uniform in shape, size and performance;

3) When the iron core is saturated, the magnetic permeability is approximately the same as that of air.

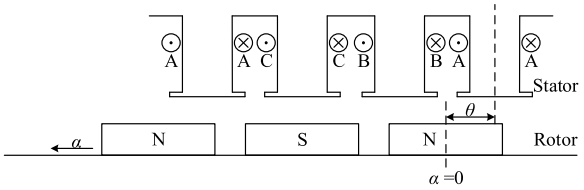

FIGURE 2. Relative position diagram of permanent magnet and armature teeth.

Fig. 2 shows the relative position of permanent magnet and armature teeth. According to the first assumption, the magnetic energy in the motor is approximately stored in the air gap and permanent magnets. And the no-load cogging torque can be calculated by the following formulas:

$$T_{cog(no-load)} \approx -\partial \left(W_{airgap} + W_{PM}\right) / (\partial\theta) = \partial \left[1/(2\mu_0) \int_V B^2(\theta,\alpha)\, dV\right] / (\partial\theta) \quad (2)$$

$$B(\theta,\alpha) = B_r(\alpha) h_m(\alpha) / [h_m(\alpha) + \delta(\theta,\alpha)] \quad (3)$$

where μ_0 is the magnetic permeability of air, $B(\theta,\alpha)$ is the air gap flux density, $B_r(\alpha)$ is the remnant flux density, $h_m(\alpha)$ is the width of permanent magnet, $\delta(\theta,\alpha)$ is the air gap length of effective magnetic circuit.

Fig. 3 shows the permeability distribution of the PMSM under different load condition. Under no-load condition, the relative permeability of the stator core is relatively high, and its distribution is uniform. Therefore, the effective air gap length δ and the no-load cogging torque are influenced by the structure of the slots. However, with the injecting of the rated-load current, the tooth-tips gradually become saturated at first and its relative permeability decreases accordingly. It means that the effective air gap length δ is also influenced by the load current. When injecting 2 times rated load, the saturation of the stator core is more significant, and the permeability of the tooth-tips is quite close to that of the air gap. Combined with (2) and (3), it is not difficult to get the conclusion that the cogging torque will change with load. In order to investigate the relationship between the cogging torque and the load, and to make it possible to reduce the cogging torque under load for further research, a calculation method for on-load cogging torque of PMSM needs to be studied.

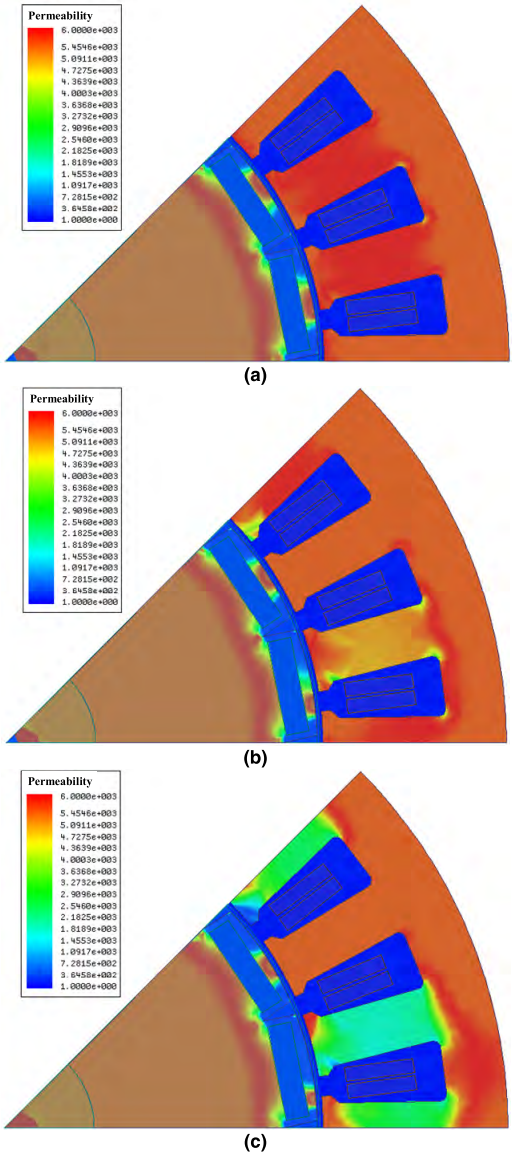

FIGURE 3. Permeability distribution. (a) No load. (b) Rated load. (c) 2 times rated load.

IV. CALCULATION METHOD

Different from the no-load condition, the components of the output torque under load condition are more complicated. The on-load output torque of PMSM usually consists of four main parts: average torque, ripple torque, reluctance torque and cogging torque, when ignoring the friction torque. On the occasion of no-load, the cogging torque can be directly obtained from the FEA. However, in the case of load, it is very difficult to calculate the cogging torque directly because of the magnetic saturation of motor cores. In order to explore the change of cogging torque with load, a calculation method for on-load cogging torque of PMSM is proposed in this paper.

Fig.4 presents a flowchart for the method to calculate the cogging torque extracted from the output torque at load operation. First, the reluctance torque can be eliminated by $i_d = 0$ control, which considering the phase delay of permanent magnet field flux. Next, the appropriate currents are injected into the stator windings, and the average torque and ripple torque are calculated. Finally, cogging torque is extracted from the output torque, which is calculated by the FEA. For the sake of clarity, a 24-slot/16-pole permanent magnet

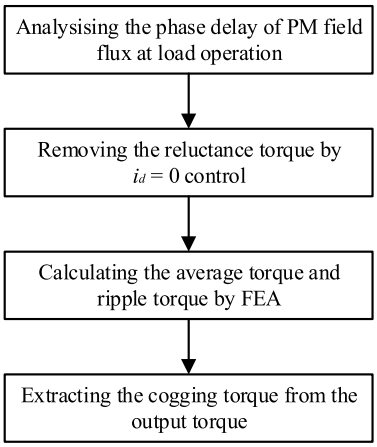

FIGURE 4. Flowchart for the proposed method.

machine is adopted to explain the process of the proposed method, and several important steps of which are described in detail in Sections IV-A–IV-C.

A. REMOVING THE RELUCTANCE TORQUE

The PMSM electromagnetic torque, in steady-state conditions, can be written as follow:

$$T_e = T_{PM} + T_r = 1.5P\varphi_{PM} i_q + 1.5P(L_d - L_q) i_d i_q \quad (4)$$

where T_{PM} is the torque caused by the permanent magnet. T_r is the reluctance torque. P is the number of pole pairs. φ_{PM} is the permanent magnet flux linkage. L_d and L_q are the d- and q-axis inductances, respectively. i_d and i_q are the d- and q-axis currents, respectively.

It can be seen from (4) that the reluctance torque is usually negligible when $i_d = 0$. However, the phase of φ_{PM} varies with load conditions according to the variation of the core saturation state. Because of the shifting of φ_{PM}, the d-axis current is not equal to zero even if using $i_d = 0$ control.

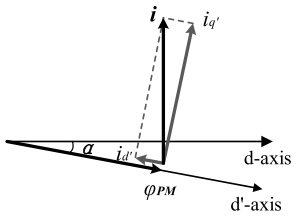

FIGURE 5. Conventional $i_d = 0$ control.

Fig. 5 shows the direction of composed current vector **i** and $\boldsymbol{\varphi}_{\mathbf{PM}}$ without considering the shifting of the permanent magnet field flux. In the figure, the permanent magnet flux linkage under load condition lags behind the no-load permanent magnet flux linkage, and the phase error is defined as α. In addition, $i_{d'}$ and $i_{q'}$ are the actual d- and q-axis current under load operation, thus the reluctance torque cannot be ignored. In order to removing the reluctance torque from the

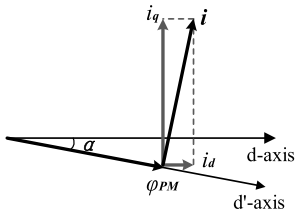

FIGURE 6. Modified $i_d = 0$ control.

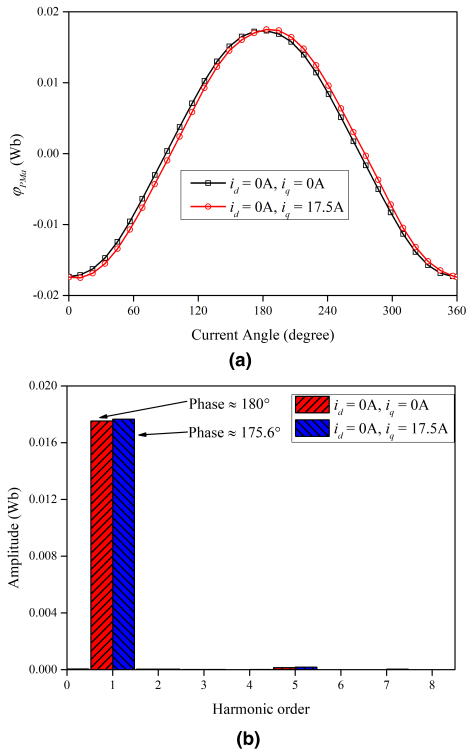

FIGURE 7. Variation of $\varphi_{\mathbf{PMa}}$ with current angle under different load condition. (a) Waveform. (b) Spectra.

output torque, the composed current vector should be perpendicular to the permanent magnet field flux by clockwise rotation. With the injection of suitable d-axis current, the d'-axis current becomes zero, as shown in Fig. 6. With this approach and not changing the size of load, the d- and q-axis currents are modified as follow:

$$\begin{cases} i_d = |\mathbf{i}| \sin\alpha \\ i_q = |\mathbf{i}| \cos\alpha \end{cases} \quad (5)$$

Fig. 7(a) shows the A-axis permanent magnet flux linkage distributions for two operating states. Compared with the no-load operation, the phase of the permanent magnet flux linkage exists an offset at rated load. In order to obtain the phase error, a fast Fourier transform (FFT) analysis is used in this paper. The harmonics of the A-axis permanent magnet flux linkage are almost non-existent, and the phase error α is about 4.4 degree, as shown in Fig.7(b). According to (5), the reluctance torque is almost eliminated at rated load with $i_d = 1.34A$, $i_q = 17.45A$.

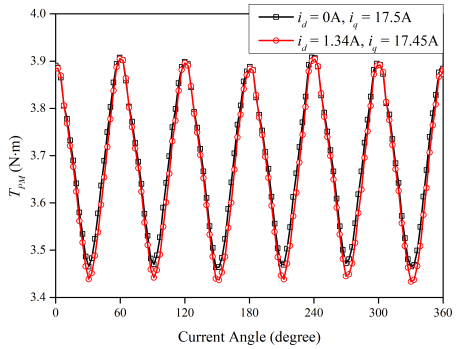

FIGURE 8. Variation of Permanent Magnet Torque with Current Angle under different load condition.

B. CALCULATING THE AVERAGE TORQUE AND RIPPLE TORQUE

The average torque and ripple torque are produced by an armature reaction field between the magnetic flux of a permanent magnet and the magnetic flux resulting from stator winding current. For convenience of calculations, the sum of the average torque and ripple torque is called the permanent magnet torque, which is shown as follow:

$$T_{PM} = T_{avg} + T_w \tag{6}$$

The flux linkage of each phase consists of the permanent magnet flux linkage component and the flux linkage caused by inductance on the load operation. Then, the permanent magnet torque can be calculated as follows:

$$\begin{cases} e_{PMa} = d(\varphi_a - L_{aa}i_a - L_{ab}i_b - L_{ac}i_c)/(dt) \\ e_{PMb} = d(\varphi_b - L_{ba}i_a - L_{bb}i_b - L_{bc}i_c)/(dt) \\ e_{PMc} = d(\varphi_c - L_{ca}i_a - L_{cb}i_b - L_{cc}i_c)/(dt) \end{cases} \tag{7}$$

$$T_{PM} = 9.55\left(e_{aPM}i_a + e_{bPM}i_b + e_{cPM}i_c\right)/n \tag{8}$$

where T_{avg} is the average torque. T_w is the ripple torque. e_{PMa}, e_{PMb} and e_{PMc} are the a-, b- and c-axis on-load back EMF. φ_a, φ_b and φ_c are total a-, b- and c-axis flux linkages, respectively. L_{aa}, L_{bb} and L_{cc} are a-, b- and c-axis self inductances, respectively. L_{ab}, L_{ac}, L_{ba}, L_{bc}, L_{ca}, L_{cb} are a-, b- and c-axis mutual inductances, respectively. i_a, i_b and i_c are a-, b- and c-axis current, respectively. n is the rotor speed.

Based on (7) and (8), the permanent magnet torque with different currents are calculated by FEA and shown in Fig. 8. It can be seen that, for each load condition, the number of fluctuations of the permanent magnet torque is 6 during one period of current waveform. The peak-to-peak value of the permanent magnet torque on $i_d = 0A$ and $i_q = 17.5A$ load is 0.44 Nm, which is slightly less than the one on $i_d = 1.34A$ and $i_q = 17.45A$ load. The reason for this phenomenon is illustrated in Section IV-A.

Because of the three-phase symmetry of the motor, this paper takes phase A as an example. The variation of e_{PMa} and i_a with current angle are shown in Fig. 9. It is revealed that the phase difference of voltage and current is zero by considering the phase delay of the permanent magnet flux linkage. The

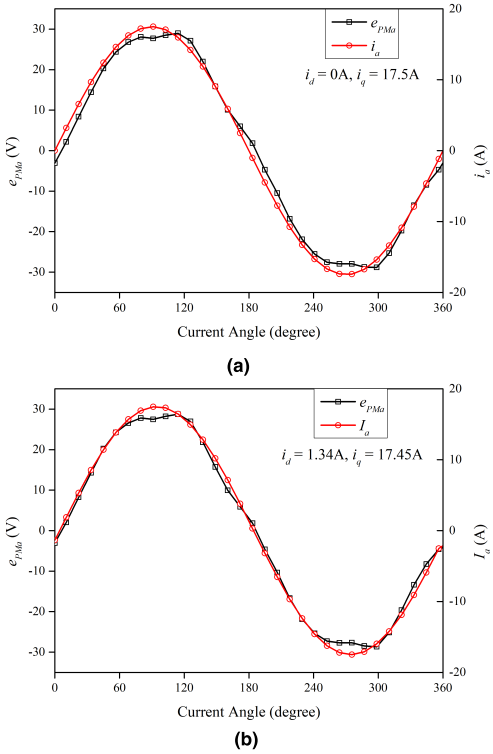

FIGURE 9. Variation of and with current angle under load condition: (a) $i_d = 0A$, $i_q = 17.5A$; and (b) $i_d = 1.34A$, $i_q = 17.45A$.

dominant harmonics of e_{PMa} are the 5th and 7th harmonic, and the FFT analysis results are shown in Fig. 10.

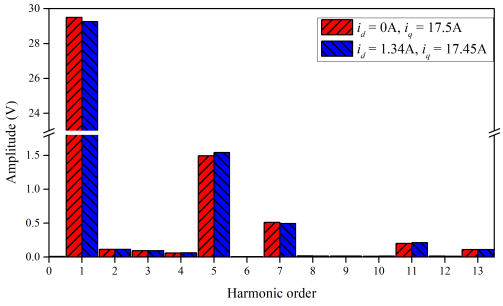

FIGURE 10. Harmonics analysis of e_{PMa} under different load condition.

For further investigation on the appearance of the fluctuations of the permanent magnet torque, e_{PMa}, e_{PMb} and e_{PMc} are expanded, which is shown as follow:

$$\begin{cases} e_{PMa} = \sum_{k=1,5,7}^{k} E_{mk}\sin(k\omega t) \\ e_{PMb} = \sum_{k=1,5,7}^{k} E_{mk}\sin(k\omega t - 1.5k\pi) \\ e_{PMc} = \sum_{k=1,5,7}^{k} E_{mk}\sin(k\omega t + 1.5k\pi) \end{cases} \tag{9}$$

where k is the harmonic order. E_{mk} is the amplitude of the k-order of the back EMF. ω is the angular frequency.

Due to the symmetrical three-phase circuit, the stator current can be written as:

$$\begin{cases} i_a = I_m \sin(\omega t) \\ i_b = I_m \sin(\omega t - 1.5\pi) \\ i_c = I_m \sin(\omega t + 1.5\pi) \end{cases} \tag{10}$$

where I_m is the amplitude of the phase current.

Substituting (9) and (10) into (8) gives

$$\begin{aligned} T_{PM} &= T_{avg} + T_w \\ &= 14.33 I_m E_{m1}/n + 14.33 I_m (E_{m7} - E_{m5}) \cos(6\omega t)/n \end{aligned} \tag{11}$$

The DC component of the permanent magnet torque is the average torque, and the AC component is the ripple torque, which are illustrated in (11) and Fig. 8. In addition, the average torque and the rippled torque can be calculated by the preceding steps.

C. EXTRACTING COGGING TORQUE FROM THE OUTPUT TORQUE

Combined with the obtained average torque and rippled torque, the cogging torque is calculated by the formula as follow:

$$T_\Delta = T_{out} - T_{PM} \tag{12}$$

where T_{out} is the output torque of motor, which may be pre-calculated by FEA. T_Δ is the remaining torque after removing permanent magnet torque in the output torque.

Since the least common multiple between the number of slots and the number of poles is 48, and the pole number of the rotor is 16, the frequency of the cogging torque waveform is 6 times as great as that of the current waveform. The variation of T_Δ with current angle and the FFT result of T_Δ are shown in Fig. 11. When $i_d = 0A$ and $i_q = 0A$, the T_Δ is equal to the open-circuit cogging torque as a result of no current in stator windings. At rated load, it can be seen from Fig. 11(b), the harmonic distribution of the T_Δ under $i_d = 0$A and $i_q = 17.5$A load is similar to that of the T_Δ under $i_d = 1.34$A and $i_q = 17.45$A load. The difference between these two load conditions is only the DC part. The DC part of the T_Δ under $i_d = 0$A and $i_q = 17.5$A load is non-zero and not negligible. The DC component is the reluctance torque caused by the magnetic saturation on the tooth of the stator core, which has been discussed in Section IV-A. The DC part of the T_Δ under $i_d = 1.34$A and $i_q = 17.45$A load is also non-zero, but it is markedly reduced. Due to the local saturation in the stator teeth of the motor, the flux linkage produced by armature current and permanent magnet flux are cross magnetized, and they have a shared magnetic circuit, which results in the DC part. Compared with the output torque, this part is very small, so it is not considered in this paper. Combined with the previous analysis, the average torque, ripple torque and reluctance torque have been calculated, which means the

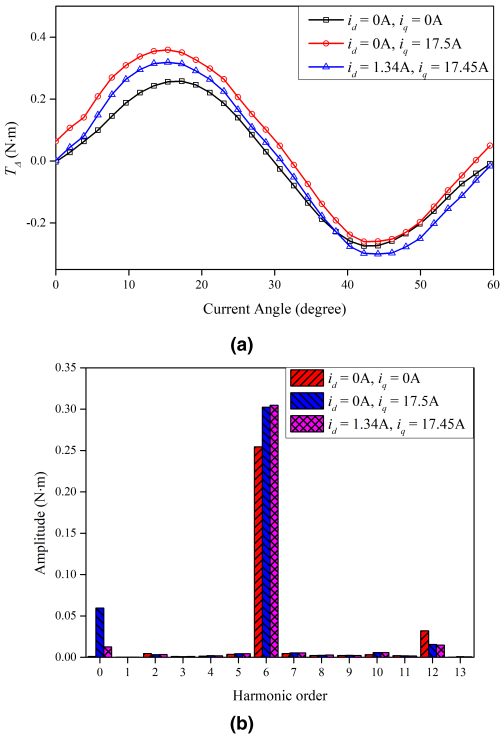

FIGURE 11. Variation of T_Δ with Current Angle under different load condition and the FFT result of T_Δ. (a) Waveform. (b) Spectra.

T_Δ is the cogging torque under rated-load condition. On this basis, it is obvious that the peak-to-peak of the rated-load cogging torque is higher than the one of the open-circuit cogging torque.

Due to the phase of stator current is used to eliminate the influence of reluctance torque, the method proposed in this paper can only measure the cogging torque under current with different amplitudes. To illustrate this situation, the torque T_Δ under no current and rated current with different phases are calculated by the method proposed in this paper Fig. 12 shows that the DC part of T_Δ changes with current phase when the rated current is injected into the stator winding. It is also noticed that the DC part of T_Δ is the smallest and negligible when the phase is 5 degree. In this paper, the reluctance torque can be eliminated by adjusting the phase of the current, which also means that the proposed on-load cogging torque calculation method is effective when the current is in a specific phase. This particular phase is obtained from the shifting angle of the permanent magnet flux linkage, which is illustrated in Section IV-A.

Similar to the rated-load condition, other load conditions are simulated by injecting appropriate currents to the stator windings. Due to the shifting of the PM flux linkage and the convenience of eliminating reluctance torque at load condition, the combination of id and iq can be obtained by (5), respectively. By using FFT, all the phase errors of fundamental component of A-axis PM flux linkage under different load conditions are shown in Fig. 13. Based on the above

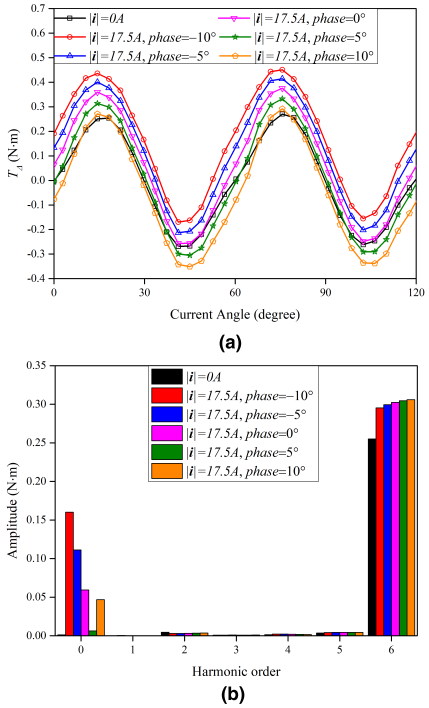

FIGURE 12. Calculated torque T_Δ obtained by the proposed method. (a) Waveform. (b) Spectra.

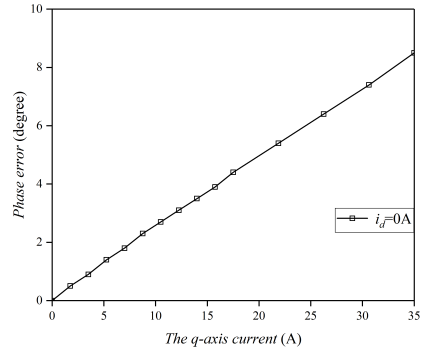

FIGURE 13. The phase errors of fundamental component of A-axis PM flux linkage under different load conditions.

results, the specific simulation currents under different load conditions are obtained in Table 2.

In order to study the relationship between the cogging torque and the saturation state of the core, the cogging torque under different loads has been calculated by the proposed method, respectively. The cogging torques of PMSM ranging from zero to full load in percentage terms are shown in Fig. 14. As the load increases, the on-load cogging torques in case of overloading are shown in Fig. 15. As can be seen from Fig. 16, the cogging torque rises with the increase of load currents. Before the actual load reaches the rated value, the peak-to-peak value of the on-load cogging torque increases slowly with load. After it reaches the rated value, due to the local magnetic saturation in tooth-tips is much stronger, the increase speed of on-load cogging torque is more rapidly with load.

TABLE 2. The specific simulation currents under different load conditions.

Load Condition	Load	Phase	Specific simulation current
No-load	$\|\boldsymbol{i}\|$ = 0A	0°	i_d = 0A, i_q = 0A
1/10 rated-load	$\|\boldsymbol{i}\|$ = 1.75A	0.5°	i_d = 0.02A, i_q = 1.75A
1/5 rated-load	$\|\boldsymbol{i}\|$ = 3.5A	0.9°	i_d = 0.06A, i_q = 3.50A
3/10 rated-load	$\|\boldsymbol{i}\|$ = 5.25A	1.4°	i_d = 0.13A, i_q = 5.25A
2/5 rated-load	$\|\boldsymbol{i}\|$ = 7A	1.8°	i_d = 0.22A, i_q = 7.00A
1/2 rated-load	$\|\boldsymbol{i}\|$ = 8.75A	2.3°	i_d = 0.35A, i_q = 8.74A
3/5 rated-load	$\|\boldsymbol{i}\|$ = 10.5A	2.7°	i_d = 0.49A, i_q = 10.49A
7/10 rated-load	$\|\boldsymbol{i}\|$ = 12.25A	3.1°	i_d = 0.66A, i_q = 12.23A
4/5 rated-load	$\|\boldsymbol{i}\|$ = 14A	3.5°	i_d = 0.85A, i_q = 13.97A
9/10 rated-load	$\|\boldsymbol{i}\|$ = 15.75A	3.9°	i_d = 1.07A, i_q = 15.71A
Rated-load	$\|\boldsymbol{i}\|$ = 17.5A	4.4°	i_d = 1.34A, i_q = 17.45A
5/4 rated-load	$\|\boldsymbol{i}\|$ = 21.88A	5.4°	i_d = 2.06A, i_q = 21.78A
3/2 rated-load	$\|\boldsymbol{i}\|$ = 26.25A	6.4°	i_d = 2.93A, i_q = 26.09A
7/4 rated-load	$\|\boldsymbol{i}\|$ = 30.63A	7.4°	i_d = 3.94A, i_q = 30.37A
2 rated-load	$\|\boldsymbol{i}\|$ = 35A	8.5°	i_d = 5.17A, i_q = 34.62A

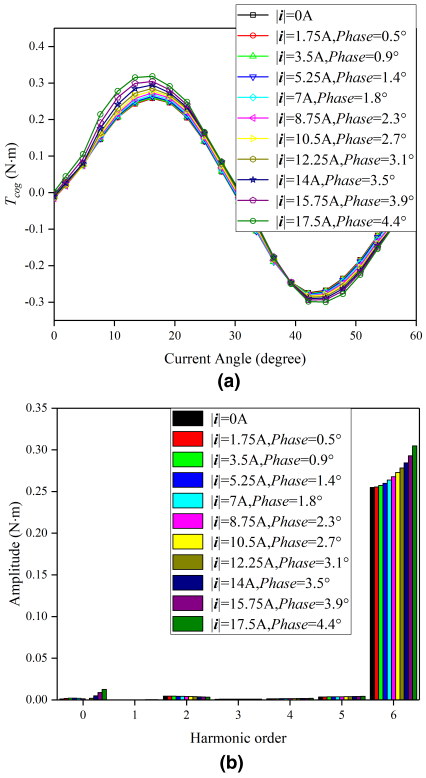

FIGURE 14. Variation of T_{cog} with Current Angle under different load conditions ranging from zero to full load. (a) Waveform. (b) Spectra.

V. EXPERIMENTAL VALIDATION

A. EXPERIMENTAL MEASUREMENT METHOD FOR COGGING TORQUE

It is difficult to directly obtain the cogging torque of the PMSM under the load condition. However, the total output torque of the motor can be easily measured by the torque sensor. In addition, combined with the calculation method

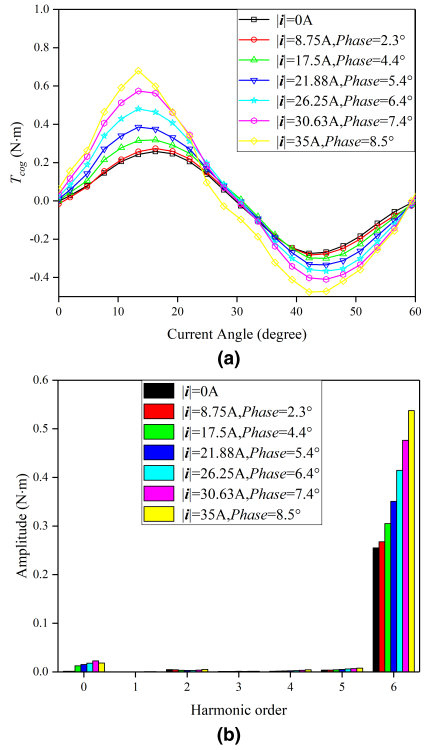

FIGURE 15. Variation of T_{cog} with Current Angle under different load conditions. (a) Waveform. (b) Spectra.

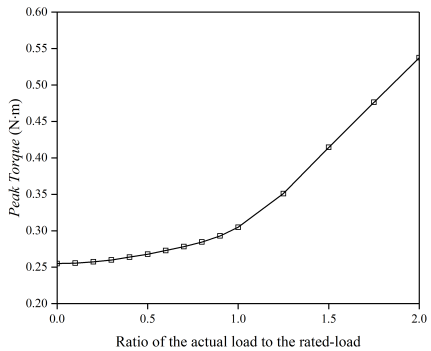

FIGURE 16. Variation of T_{cog} with Current Angle under different load condition. (a) The waveforms of the cogging torque. (b) The peak-to-peak values of the cogging torque.

of on-load cogging torque under load conditions proposed in Sections IV, it can be found that the AC component of the output torque of the motor is mainly composed of ripple torque and cogging torque. Due to the structure of pole and slot number of the motor used in this paper, the period number of ripple torque and cogging torque are the same, which means the output torque can be shown as follows:

$$\boldsymbol{T}_{outAC} = \boldsymbol{T}_w + \boldsymbol{T}_{cog} \tag{13}$$

where $\boldsymbol{T}_{outAC}$ is the AC component of output torque vector. $\boldsymbol{T}_w$ is the ripple torque vector. $\boldsymbol{T}_{cog}$ is the cogging torque vector.

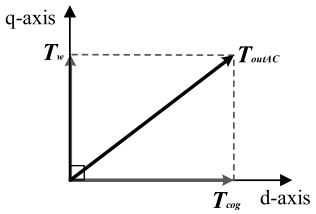

FIGURE 17. Orthogonal decomposition of the AC component of output torque.

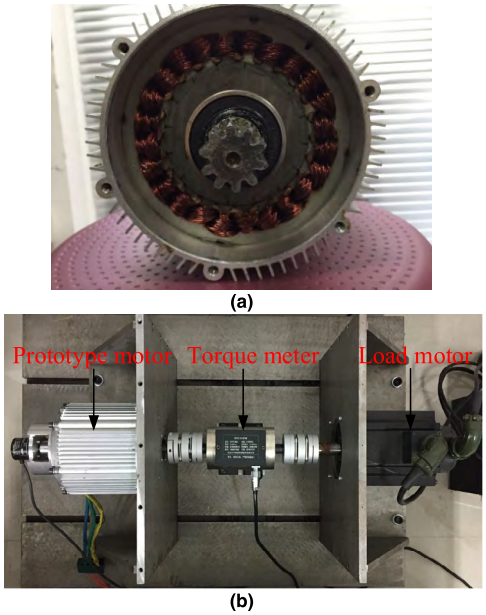

FIGURE 18. (a) Prototype motor. (b) experimental setup.

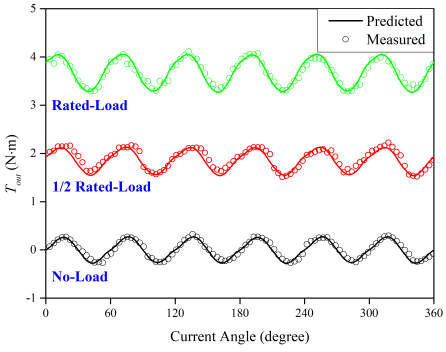

FIGURE 19. Comparison of measured and predicted output torque.

According to (10) and (11), the phase of ripple torque is 90 degrees ahead of that of cogging torque, which means that the cogging torque vector direction is the same as the d axis and the ripple torque vector direction is the same as the q axis. Therefore, the AC component of output torque can be decomposed orthogonally in Fig. 17.

It can be seen from Fig. 17 that the cogging torque can be obtained by orthogonal decomposition of the $\boldsymbol{T}_{outAC}$ on the d-q axis to remedy the lack of experimental measurement.

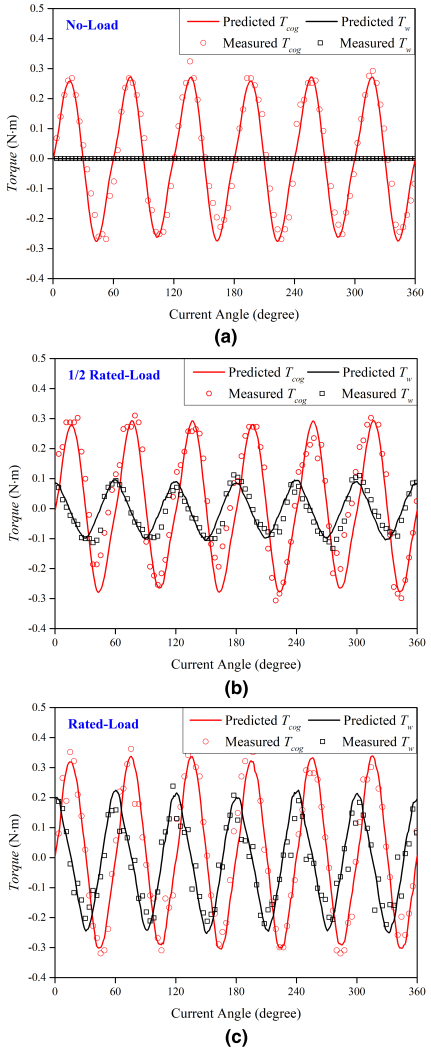

FIGURE 20. The comparison of predicted and measured torque. (a) No-load. (b) 1/2 Rated-load. (c) Rated-load.

B. EXPERIMENTAL VALIDATION

A prototype motor, whose parameters are consistent with the analysis model, has been manufactured to verify the effectiveness of the proposed separation method. Fig. 18 shows the photographs of the prototype motor and the experimental setup. The experimental setup is composed of three devices: the prototype motor, the servo motor and the torque meter. The torque meter achieves high accuracy, the static precision of the sensor is 0.5% N·m, and the measurement range is about ± 5 N·m. The rated speed of the prototype motor is 2000 rpm in this paper. Because the sampling frequency of the torque meter is relatively low, the data collected by the sensor cannot restore the torque waveform well when the prototype motor works at the rated speed. In addition, the lower the speed of the prototype motor, the better the torque waveform can be obtained. Therefore, the servo motor is used to run in the speed control mode to ensure that the prototype motor can run at a low and uniform speed. What's more, the lowest set speed of servo motor is 1 rpm, so the torque measurement experiments in this paper are all carried out with the speed of 1 rpm. The prototype motor operates in the constant torque mode, and the servo motor operates in the speed mode. The direction of the torque and the speed is the same. In this operating state, the servo motor is equivalent to the mechanical load of the prototype motor. By means of FOC, the value of mechanical load can be simulated by setting the d- and q- axis current of the motor.

The comparison of predicted and measured output torque is shown in Fig. 19, and the result shows a great agreement, which can verify the validity of the simulation model. In addition, the measured cogging torque is obtained by the method illustrated in Section V-A, and the comparisons of measured and predicted torque are shown in Fig. 20. Due to the limited sensor accuracy and manufacture errors, the peak-to-peak value of the measured cogging torque and ripple torque slightly differs from the one of the predicted torque. However, the measured waveforms show similar variation trend with the predicted one. It can be also seen that ripple torque and cogging torque increase with the increase of load. From these results, the experiments validate the calculation method for on-load cogging torque of PMSM.

VI. CONCLUSION

In this paper, a calculation method for on-load cogging torque in PMSM has been proposed. The finite element analysis and field-oriented control contribute to the method, which the cross magnetization has been taken into account, and the reluctance torque is eliminated by changing the phase of the current. In addition, the average torque and the ripple torque are calculated by FEA, and thus the on-load cogging torque is separated from the output torque. What's more, the experimental measurement method of cogging torque of PMSM is also introduced in this paper. Although the proposed method is only effective when the current is in a specific phase, the proposed method requires fewer FE calculations and is convenient to implement compared with the existing methods. It is used to calculate the cogging torque of 24 slots and 16 poles PMSM under different load conditions, and the results show the change rule of cogging torque with load. The calculation method has been verified by the simulations and the experiments. The methods reported here will open up avenues for reducing the on-load cogging torque and torque ripple in the further research.

REFERENCES

[1] S. Morimoto, "Trend of permanent magnet synchronous machines," *IEEJ Trans. Elect. Electron. Eng.*, vol. 2, no. 3, pp. 101–108, 2010.
[2] K. Wang, H. Sun, L. Zhang, C. Liu, and Z. Zhu, "An overview of rotor pole optimization techniques for permanent magnet synchronous machines," *Proc. Chin. Soc. Elect. Eng.*, vol. 37, no. 24, pp. 7304–7317, 2017.
[3] W. Q. Chu and Z. Q. Zhu, "Investigation of torque ripples in permanent magnet synchronous machines with skewing," *IEEE Trans. Magn.*, vol. 49, no. 3, pp. 1211–1220, Mar. 2013.
[4] X. Ge, Z. Q. Zhu, G. Kemp, D. Moule, and C. Williams, "Optimal step-skew methods for cogging torque reduction accounting for three-dimensional effect of interior permanent magnet machines," *IEEE Trans. Energy Convers.*, vol. 32, no. 1, pp. 222–232, Mar. 2017.

[5] T. Liu, S. Huang, J. Gao, and K. Lu, "Cogging torque reduction by slot-opening shift for permanent magnet machines," *IEEE Trans. Magn.*, vol. 49, no. 7, pp. 4028–4031, Jul. 2013.

[6] D.-H. Wang, X.-H. Wang, T.-T. Ding, Y.-B. Yang, R. Zhang, and S.-Y. Liu, "Optimization for the asymmetric angles of magnetic pole to reduce cogging torque in inner-buried PM brushless DC motors," *Proc. Chin. Soc. Elect. Eng.*, vol. 28, no. 3, pp. 66–70, 2008.

[7] Z. Guofu, W. Qiya, Y. Wenying, and L. Huimin, "Permanent-magnet equivalent model of calculating relay's static attractive torque characteristics by finite element method," *IEEE Trans. Magn.*, vol. 48, no. 9, pp. 2467–2471, Sep. 2012.

[8] L. Zhu, S. Z. Jiang, Z. Q. Zhu, and C. C. Chan, "Analytical methods for minimizing cogging torque in permanent-magnet machines," *IEEE Trans. Magn.*, vol. 45, no. 4, pp. 2023–2031, Apr. 2009.

[9] C. M. Spargo, B. C. Mecrow, and J. D. Widmer, "A seminumerical finite-element postprocessing torque ripple analysis technique for synchronous electric machines utilizing the air-gap Maxwell stress tensor," *IEEE Trans. Magn.*, vol. 50, no. 5, pp. 1–9, May 2014.

[10] E.-P. Zhang and K. Shi, "Cogging torque analysis for permanent magnetic motors using Maxwell Tensor," *Small Special Elect. Mach.*, vol. 38, no. 3, pp. 27–30, 2010.

[11] X. Wang, Y. Yang, and D. Fu, "Study of cogging torque in surface-mounted permanent magnet motors with energy method," *J. Magn. Magn. Mater.*, vol. 267, no. 1, pp. 80–85, Nov. 2003.

[12] L. J. Wu, Z. Q. Zhu, D. A. Staton, M. Popescu, and D. Hawkins, "Comparison of analytical models of cogging torque in surface-mounted PM machines," *IEEE Trans. Ind. Electron.*, vol. 59, no. 6, pp. 2414–2425, Jun. 2012.

[13] C. Xia, Z. Chen, T. Shi, and H. Wang, "Cogging torque modeling and analyzing for surface-mounted permanent magnet machines with auxiliary slots," *IEEE Trans. Magn.*, vol. 49, no. 9, pp. 5112–5123, Sep. 2013.

[14] Y. Huang, J. Dong, J. Zhu, and Y. Guo, "Core loss modeling for permanent-magnet motor based on flux variation locus and finite-element method," *IEEE Trans. Magn.*, vol. 48, no. 2, pp. 1023–1026, Feb. 2012.

[15] K.-C. Kim, "A novel method for minimization of cogging torque and torque ripple for interior permanent magnet synchronous motor," *IEEE Trans. Magn.*, vol. 50, no. 2, pp. 793–796, Feb. 2014.

[16] G.-J. Park, Y. J. Kim, and S.-Y. Jung, "Design of ipmsm applying V-shape skew considering axial force distribution and performance characteristics according to the rotating direction," *IEEE Trans. Appl. Supercond.*, vol. 26, no. 3, Jun. 2016, Art. no. 0605205.

[17] D. Wang, X. Wang, D. Qiao, Y. Pei, and S.-Y. Jung, "Reducing cogging torque in surface-mounted permanent-magnet motors by nonuniformly distributed teeth method," *IEEE Trans. Magn.*, vol. 47, no. 9, pp. 2231–2239, Sep. 2011.

[18] I. Petrov, P. Ponomarev, Y. Alexandrova, and J. Pyrhönen, "Unequal teeth widths for torque ripple reduction in permanent magnet synchronous machines with fractional-slot non-overlapping windings," *IEEE Trans. Magn.*, vol. 51, no. 2, Feb. 2015, Art. no. 8100309.

[19] G. J. Li, B. Ren, Z. Q. Zhu, Y. X. Li, and J. Ma, "Cogging torque mitigation of modular permanent magnet machines," *IEEE Trans. Magn.*, vol. 52, no. 1, Jan. 2016, Art. no. 8100210.

[20] S. L. Ho, N. N. Chen, and W. N. Fu, "An optimal design method for the minimization of cogging torques of a permanent magnet motor using FEM and genetic algorithm," *IEEE Trans. Appl. Supercond.*, vol. 20, no. 3, pp. 861–864, Jun. 2010.

[21] B. Peng, W. Zhao, and X. Wang, "The method for reducing intrinsic shaft voltage by suitable selection of pole-arc coefficient in fractional-slot permanent-magnet synchronous machines," *IEEE Trans. Magn.*, vol. 54, no. 11, Nov. 2018, Art. no. 8109805.

[22] R. Lateb, N. Takorabet, and F. Meibody-Tabar, "Effect of magnet segmentation on the cogging torque in surface-mounted permanent-magnet motors," *IEEE Trans. Magn.*, vol. 42, no. 3, pp. 442–445, Mar. 2006.

[23] W. Ren, Q. Xu, Q. Li, and L. Zhou, "Reduction of cogging torque and torque ripple in interior PM machines with asymmetrical V-type rotor design," *IEEE Trans. Magn.*, vol. 52, no. 7, Jul. 2016, Art. no. 8104105.

[24] W. Q. Chu and Z. Q. Zhu, "Average torque separation in permanent magnet synchronous machines using frozen permeability," *IEEE Trans. Magn.*, vol. 49, no. 3, pp. 1202–1210, Mar. 2013.

[25] K. Abbaszadeh and F. R. Alam, "On-load field component separation in surface-mounted permanent-magnet motors using an improved conformal mapping method," *IEEE Trans. Magn.*, vol. 52, no. 2, Feb. 2016, Art. no. 5200112.

[26] Z. Azar, Z. Q. Zhu, and G. Ombach, "Influence of electric loading and magnetic saturation on cogging torque, back-EMF and torque ripple of PM machines," *IEEE Trans. Magn.*, vol. 48, no. 10, pp. 2650–2658, Oct. 2012.

[27] K.-H. Shin, J.-Y. Choi, and H.-W. Cho, "Characteristic analysis of interior permanent-magnet synchronous machine with fractional-slot concentrated winding considering nonlinear magnetic saturation," *IEEE Trans. Appl. Supercond.*, vol. 26, no. 4, Jun. 2016, Art. no. 5200404.

[28] G. D. Feng, C. Lai, and N. C. Kar, "A novel current injection-based online parameter estimation method for PMSMs considering magnetic saturation," *IEEE Trans. Magn.*, vol. 52, no. 7, Jul. 2016, Art. no. 8106004.

[29] D. Wu and Z. Q. Zhu, "On-load voltage distortion in fractional slot surface-mounted permanent magnet machines considering local magnetic saturation," *IEEE Trans. Magn.*, vol. 51, no. 8, Aug. 2015, Art. no. 8106410.

[30] D. Wu, Z. Q. Zhu, and W. Chu, "Reduction of on-load terminal voltage distortion in fractional slot interior permanent magnet machines," *IEEE Trans. Energy Convers.*, vol. 31, no. 3, pp. 1161–1169, Sep. 2016.

[31] D. Wu and Z. Q. Zhu, "Design tradeoff between cogging torque and torque ripple in fractional slot surface-mounted permanent magnet machines," *IEEE Trans. Magn.*, vol. 51, no. 11, Nov. 2015, Art. no. 8108704.

[32] W. Q. Chu and Z. Q. Zhu, "Reduction of on-load torque ripples in permanent magnet synchronous machines by improved skewing," *IEEE Trans. Magn.*, vol. 49, no. 7, pp. 3822–3825, Jul. 2013.

[33] K. Yamazaki and M. Kumagai, "Torque analysis of interior permanent-magnet synchronous motors by considering cross-magnetization: Variation in torque components with permanent-magnet configurations," *IEEE Trans. Ind. Electron.*, vol. 61, no. 7, pp. 3192–3201, Jul. 2014.

[34] K.-C. Kim and S.-H. Jeon, "Analysis on correlation between cogging torque and torque ripple by considering magnetic saturation," *IEEE Trans. Magn.*, vol. 49, no. 5, pp. 2417–2420, May 2013.

[35] W. Q. Chu and Z. Q. Zhu, "On-load cogging torque calculation in permanent magnet machines," *IEEE Trans. Magn.*, vol. 49, no. 6, pp. 2982–2989, Jun. 2013.

[36] A. Hanic, D. Žarko, D. Kuhinek, and Z. Hanic, "On-load analysis of saturated surface permanent magnet machines using conformal mapping and magnetic equivalent circuits," *IEEE Trans. Energy Convers.*, vol. 33, no. 3, pp. 915–924, Sep. 2018.

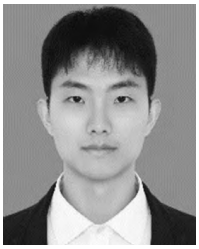

WEIYE WANG was born in Huai'an, Jiangsu, China, in 1994. He received the B.S. degree in electrical engineering from Nanjing Normal University, in 2016, where he is currently pursuing the degree with the Electrical Engineering Department, School of Electrical and Automation.

His research interest includes high-performance control methods of permanent magnet synchronous motor.

HUI MA was born in Yangzhou, Jiangsu, China, in 1995. She received the B.S. degree in electrical engineering from Nanjing Xiaozhuang University, in 2017. She is currently pursuing the degree with the Electrical Engineering Department, School of Electrical and Automation, Nanjing Normal University.

Her research interest includes permanent magnet synchronous motor design.

XIN QIU was born in Huai'an, Jiangsu, China, in 1985. He received the B.S., M.S., and Ph.D. degrees in electrical engineering from the Nanjing University of Aeronautics and Astronautics, in 2007, 2010, and 2014, respectively.

Since 2014, he has been an Associate Professor with the Electrical Engineering Department, School of Electrical and Automation, Nanjing Normal University. He has authored more than 12 articles, and more than ten inventions. He has presided over and participated in more than ten National Key Research and Development Projects, National Natural Science Foundation Projects, Jiangsu Science and Technology Innovation and Achievement Transformation (major science and technology support) Projects, and Jiangsu Science and Technology Support Key Projects. His research interests include the design of permanent magnet motor and high performance control, 3D printing control systems, and electric vehicle electric drive systems.

JIANFEI YANG was born in Nantong, Jiangsu, China, in 1982. He received the B.S. and Ph.D. degrees in electrical engineering from the Nanjing University of Aeronautics and Astronautics, in 2005 and 2011, respectively.

Since 2017, he has been an Associate Professor with the Electrical Engineering Department, School of Electrical and Automation, Nanjing Normal University. He has authored two books, more than 13 articles, and more than 5 inventions. He has presided over and participated in more than National and Provincial Scientific Research Projects, including National Natural Science Foundation of China, Natural Science Foundation of Jiangsu Province, and Jiangsu Province Industry-University-Research Forward-looking Joint Research Project. His research interest includes high-performance

control methods of power electronics and power transmission, permanent magnet synchronous motor, and 3D printing (rapid prototyping technology).

He was a recipient of the Award of the Jiangsu Province ''Six-Talent-Peak'' Project, in 2017, and the title of ''Blue-Project'' Young Backbone Teacher of Nanjing Normal University.